Nanoscale

Accepted Manuscript

This article can be cited before page numbers have been issued, to do this please use: C. Dohno, S. Makishi, K. Nakatani and S. Contera, *Nanoscale*, 2017, DOI: 10.1039/C6NR07084A.

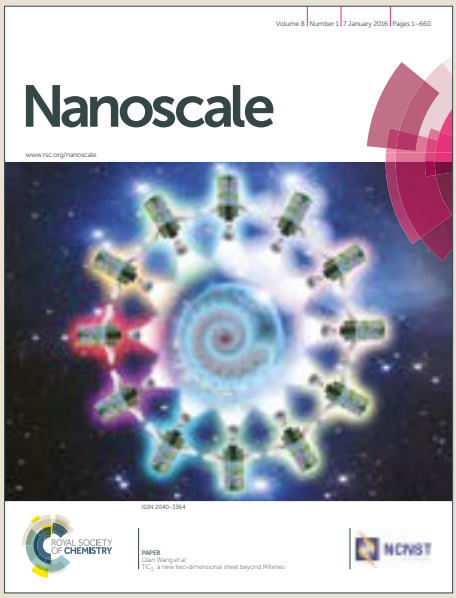

ROYAL SOCIETY OF CHEMISTRY

rsc.li/nanoscale

ROYAL SOCIETY OF CHEMISTRY
View Article Online
DOI: 10.1039/C6NR07084A

Journal Name

ARTICLE

Amphiphilic DNA tiles for controlled insertion and 2D assembly on fluid lipid membranes: Effect on mechanical properties.

Received 00th January 20xx,
Accepted 00th January 20xx

DOI: 10.1039/x0xx00000x

www.rsc.org/

Chikara Dohno,[a,b,*] Shingo Makishi,[a] Kazuhiko Nakatani,[a] and Sonia Contera,[c,*]

Future lipid membrane-associated DNA nanostructures are expected to find applications ranging from synthetic biology to nanomedicine. Here we have designed and synthesized DNA tiles and modified them by amphiphilic covalent moieties. dod-DEG groups, which consist of a hydrophilic diethylene glycol (DEG) and a hydrophobic dodecyl group, are introduced at the phosphate backbone to create amphiphilic DNA strands which are subsequently introduced into one face of DNA tiles. In this way the tile becomes able to stably bind to lipid membranes by insertion of the hydrophobic groups inside the bilayer core. The functionalized tiles do not aggregate in solution. Our results show that these amphiphilic DNA tiles can bind and assemble into 2D lattices on both gel and fluid lipid bilayers. The binding of the DNA structures to membranes is dependent on the lipid phase of the membrane, the concentration of Mg^{2+} cation, the length of the amphiphilic modifications to the DNA as well as on the density of the modifications within the tile. Atomic force microscopy–based force spectroscopy is used to investigate the effect of the inserted DNA tiles on the mechanical properties of the lipid membranes. The results indicate that the insertion of DNA tiles produces an approx. 20% increase of the bilayer breakthrough force.

Introduction

The intense activity of the field of DNA nanotechnology over the last decades has made it possible to construct almost any arbitrary shape at the nanoscale using DNA as a building block.[1–6] However DNA nanotechnology still does not achieve an important structural feature: multiscale organization and compartmentalization; in biological systems these tasks are mainly carried out by lipids. In living cells lipid bilayers define the boundaries of the cell organelles and of the cell itself. By creating boundaries and interfaces membranes also focus the action of signaling systems that can take advantage of the membrane interface to compartmentalize both the substrates and products of signaling enzymes. The membrane itself is also compartmentalized; cellular plasma membranes contain combinations of lipids and proteins that can self-organize in microdomains.[7-10] These membrane microdomains may modulate and steer cellular processes by serving as organizing centers for the assembly of signaling molecules, influencing membrane fluidity and membrane protein trafficking, and regulating neurotransmission and receptor trafficking and are key to fundamental biological processes in health and disease. In specific cellular events such as autophagy, the cell can create relatively large lipid-protein assemblies such as the autophagic membrane-scaffold, a two-dimensional protein mesh linked to the membrane that mediates the mechanism to degrade bulk cytoplasmic components.[10]

It is therefore interesting both from the point of view of nanomedicine and of synthetic biology to create DNA structures that are able to interact with lipid structures.[11–13] For instance it is conceivable that DNA structures could be created that would interact with the lipid membranes of living cells, targeting specific functional domains in drug-delivery applications; DNA structures could be designed to act as nanoscale-*handles* on the cell surface that could be activated by external signals. Lipid-DNA hybrid structures could also be used to create bio-inspired enzymatic reaction assemblies separating the oxidation and reduction process into two separate chambers, or to mediate events such as vesicle docking and fusion and selective partitioning of molecules into phase-separated membranes.[11–18]

DNA structures that can attach to lipid membranes through electrostatic or hydrophobic interactions have been created in the past.[13–18] Unmodified DNA origami structures able to electrostatically bind to zwitterionic phosphatidylcholine (PC) lipid bilayers in the presence of divalent cations, Mg^{2+} and Ca^{2+} ions, have been reported.[11,15–17,19] The functionalization of the structures with hydrophobic anchors made them more stably immobilized on the membranes.[17–26] One of the first examples of the functionalized DNA nanostructure was a DNA-based hexagon able to bind to DOPC liposomes with diameters of ≈ 100 nm via porphyrin anchors.[17,18] The mobility of DNA

[a] Department of Regulatory Bioorganic Chemistry, The Institute of Scientific and Industrial Research (ISIR), Osaka University, Osaka, Ibaraki 567-0047, Japan.
[b] PRESTO, Japan Science and Technology Agency, 4-1-8 Honcho Kawaguchi, Saitama 332-0012, Japan.
[c] Clarendon Laboratory, Physics Department, University of Oxford, Oxford, OX1 3PU, UK.

Electronic Supplementary Information (ESI) available: See DOI: 10.1039/x0xx00000x

hexagons was affected by the number and position of the hydrophobic anchors. Chemically modified DNA structures that insert themselves in lipid membranes creating artificial transmembrane channels have been reported.[22,23] Czogalla et al.[19] reported the assembly of origami six-helix bundle (6HB) structures on lipids; in the absence of divalent ions, cholesterol-functionalized 6HBs were found to preferentially bind to the disordered phase of phase separated giant unilamellar vesicles, while upon addition of Mg^{2+} the helix bundles migrated into the ordered phase. DNA origami structures functionalized with cholesterol moieties were able to assemble into triskelion homotrimers and further assembled into weakly ordered arrays of hexagons and pentagons, which resembled the geometry of clathrin-coated pits.[24] 100 nm unilamellar vesicles, where liposome self-assembly was nucleated and confined inside rigid DNA nanotemplates, were reported by Yang et al.[25] DNA was used to tightly wrap unilamellar lipid vesicles, mimicking the morphology of enveloped virus particles.[26]

In contrast to solid supports, DNA-based nanostructures can in principle dynamically assemble and disassemble when they associate with lipid membranes equivalently to membrane-bound protein complexes in biology. Conversely, DNA nanostructures may also influence membrane structure and mechanical properties mimicking the effect of membrane proteins or mechanically active lipids. In this context, the mobility of the DNA nanostructures is important: they can *e.g.* stay attached to the lipids, diffuse, or form segregated structures.

Crucially for many of the applications hinted above such as DNA controlled fusion/division of compartments, or control the diffusion of structures within the membrane, more sophisticated control of membrane properties and a quantitative knowledge of the mechanical properties of these structures will be required. The effect of DNA structures on the mechanical properties of lipid membranes such as stiffness or bilayer rupture force has not been reported to date.

Here we construct chemically modified DNA tiles that are able to strongly bind to lipid membranes through an especially designed hydrophobic tail, in a controllable and stable manner and demonstrate that they remain capable of assembly in 2D structures. Tiles are interesting for this application because they are simple and easy to design, they require a small amount of DNA sequences and are easy to synthesize, and they are able to assemble into big periodic structures. Their structure and assembly/disassembly on lipid membranes is studied using the atomic force microscope (AFM) in solution. The density and length of the hydrophobic tags and the effect of the concentration of Mg^{2+} ions on the insertion and assembly is systematically assessed. Finally the effect of the tiles of the mechanical properties of the lipid membrane is investigated by AFM nanoindentation experiments.

Results and discussion

Design and synthesis of amphiphilic DNA

The strategy to create amphiphilic DNA tiles is based on previous work where we fabricated dod-modified DNA, containing hydrophobic dodecyl phosphotriester linkages as hydrophobic anchors.[27–30] The binding affinity of these dod-DNA molecules to lipid membranes depends on which part of the sequence is modified: hydrophobic modification at the end of the DNA helix resulted in more favorable binding than modifications in the middle of the helix. Here, in order to

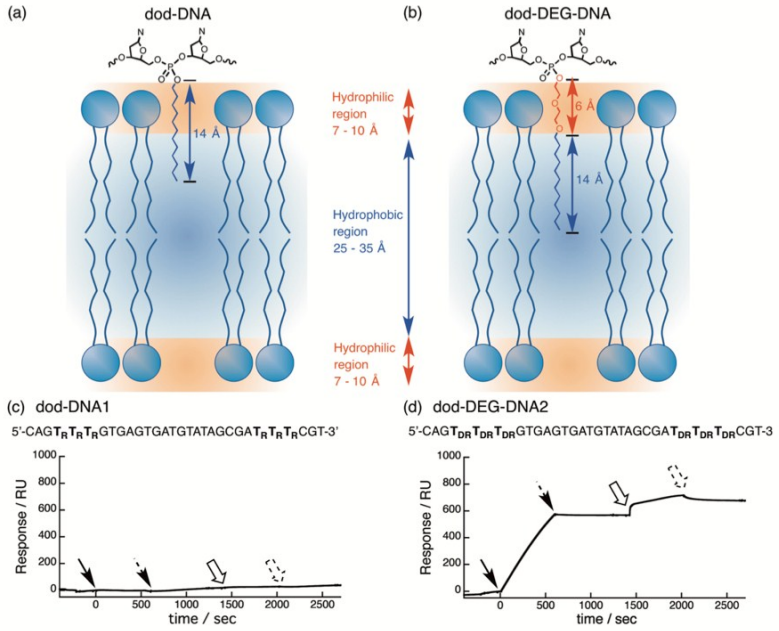

Fig. 1. (a, b) Schematic illustration of expected binding modes of (a) dod-DNA and (b) dod-DEG-DNA to a lipid membrane. "N" represents nucleobases. (c, d) SPR sensorgrams for dod-DNA and dod-DEG-DNA binding to POPC membrane. POPC vesicles were immobilized on the SPR sensor chip, followed by injections (t = 0, black solid arrows) of (c) dod-DNA1 or (d) dod-DEG-DNA2 and the complementary DNA (t = 1400, white arrows). Dashed arrows indicate the beginning of running buffer injection (washing steps, t = 600 and 1200). Dodecyl and dod-DEG triester linkage are indicated by the subscripts "R" and "DR", respectively.

improve the binding properties of dod-DNA molecules, we have synthesized a new amphiphilic DNA that specifically takes into account the lipid bilayer structure. Typically, lipid bilayers consist of a 25–35 Å hydrophobic core and a hydrophilic interface with the water solution environment composed of fully hydrated headgroups ~ 7–10 Å in thickness.[31] Assuming that dod-DNA binds to the surface of the lipid bilayer (**Fig. 1a**), the dodecyl group (ca. 14 Å) is too short to interact efficiently with the inner hydrophobic core and therefore there will be a polarity mismatch between the hydrophobic dodecyl groups and hydrophilic part of the membrane. We have designed a new amphiphilic dod-DEG-DNA molecule where a hydrophilic diethylene glycol (DEG) linkage is inserted between the hydrophobic dodecyl group and DNA backbone (**Fig. 1b**).[19,32,33] The amphiphilic dod-DEG groups (ca. 20 Å) are expected to increase the binding affinity to lipid membranes. Although the dodecyl group is still shorter than the aliphatic chains in POPC, we selected the dodecyl group to minimize the unfavorable hydrophobic interactions between the attached tails leading to aggregation of the DNAs.[28-30] Synthesis of dod-DEG-DNA was done using a previously reported procedure,[27,30] where nucleoside phosphoramidites containing a dod-DEG group were synthesized and introduced into DNA by a standard solid phase synthesis protocol (Supporting Information, **Scheme S1**).

Using this procedure we have synthesized amphiphilic DNAs that have two separate hydrophobic regions (dod-DNA1, dod-DEG-DNA2) (**Fig. 1 c, d**). Binding of the dod-DEG-DNA and dod-DNA to 1-palmitoyl-2-oleoyl-*sn*-glycero-3-phosphocholine (POPC) fluid lipid membrane was evaluated by surface plasmon resonance (SPR) with a sensor chip (L1, Biacore) functionalized with POPC vesicles.[34,35] As shown in **Fig. 1c**, SPR response indicates absence of binding of dod-DNA1. This result is expected, since dod groups introduced in the middle of DNA helix are not effective for lipid membrane binding.[28] In contrast, the SPR experiment for dod-DEG-DNA2 (**Fig. 1d**) shows efficient binding to the lipid membrane. Dissociation of the membrane-bound dod-DEG-DNA2 from the membrane surface was not observed under these conditions. Subsequent injection of the complementary DNA gave a further increase of the SPR response (**Fig. 1d**, white arrow, t = 1400 s), which indicates that hybridization with the complementary DNA strand proceeds on the membrane. These results clearly show that the dod-DEG group, even when it is introduced in the middle of the DNA helix, is effective for binding to lipid membranes.

Amphiphilic DNA tiles for 2D assembly on fluid and gel phase lipid membranes

Following the work by Seeman *et al.* where two separate units (A and B) are designed to self-assemble into a 2D DNA periodic lattice,[36] we fabricated A and B tiles where one face of the A unit was modified with two dod-DEG groups, so that the DNA tile containing dod-DEG-A units is able to bind to the lipid membrane (**Fig. 2a, and S1**). Formation of the DNA tiling lattice was confirmed by agarose gel electrophoresis (**Fig. S2**) and high resolution AFM imaging recorded on a mica surface in solution where the structure of the tiles was visible down to the smallest details (**Fig. 2b**). Both unmodified and modified DNA tiles provided similar AFM images (**Fig. 2b** and **c**). Since the B-unit has a protruding feature made of a hairpin structure,

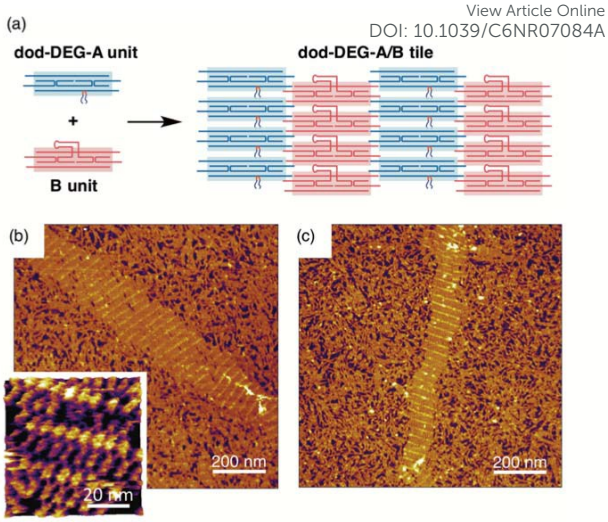

Fig. 2. (a) Scheme of the formation of DNA tiling lattice. (b) AFM images of DNA tile A/B assembled tiles on a mica surface. High resolution image is shown in the inset. (c) dod-DEG-A/B tile on mica. The images were recorded in 10 mM Tris-HCl (pH 8.0) buffer containing 12.5 mM Mg^{2+}.

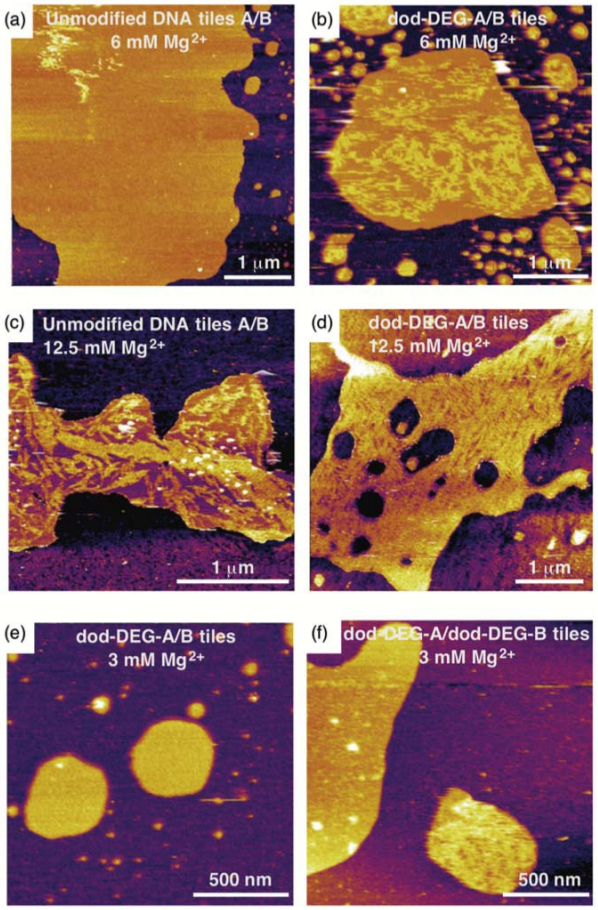

Fig. 3. AFM images of DNA tiles adsorbed on fluid POPC lipid membranes. Unmodified DNA tile A/B (a, c), dod-DEG-A/B tiles (b, d, e), or dod-DEG-A/dod-DEG-B tiles (f) were used for the measurements. These images were taken in 10 mM Tris-HCl (pH 8.0) buffer containing different concentrations of Mg^{2+}: (a, b) 6 mM Mg^{2+}; (c, d) 12.5 mM Mg^{2+}; (e, f) 3 mM Mg^{2+}. Scale bars as indicated in the images.

View Article Online
DOI: 10.1039/C6NR07084A

the assembled tiles should provide a stripe pattern with constant width on the surface.[36] Height cross-section analysis provided an average distance between the stripes of 31.4 ± 0.2 and 30.4 nm ± 0.3 for the DNA tile A/B and dod-DEG-A/B tile, respectively, which agree with the estimated spacing of 31.6 nm.

We note that dod-DEG DNA tiles could be prepared simply by single mixing of all DNAs including dod-DEG DNAs. Regardless of the presence and absence of dod-DEG modification, we could construct DNA tiles while avoiding aggregation as shown in **Fig. 2** and **S2** (AFM and gel). In contrast it has been reported that cholesterol-modified structures have a strong tendency to form aggregates in aqueous solutions due to their hydrophobic interactions and that this bring challenges to the fabrication of the cholesterol modified DNA structures.[24] This is a significant advantage of our constructs.

Binding and assembly of the 2D-periodic DNA tiling lattice on planar lipid bilayer membranes were investigated by small-amplitude amplitude modulation (AM)-AFM in solution (**Fig. 3**). Fluid POPC planar bilayers were deposited on mica, and then DNA tiles were added to the solution in the presence of divalent Mg^{2+} cations. Unmodified A/B DNA tiles (without dod-DEG) did not adsorb onto POPC bilayers at 6 mM Mg^{2+} (**Fig. 3a, S3a**). However, when the A unit was replaced by the dod-DEG-A unit, the DNA tile consisting of dod-DEG-A and unmodified B units (dod-DEG-A/B) was assembled to produce 2D DNA structures directly on the membrane surface (**Fig. 3b, S3b**). The effective binding of DNA tiles is dependent not only on the hydrophobic modification but also concentration of Mg^{2+}. At high concentration of Mg^{2+} (12.5 mM), both dod-DEG modified and unmodified DNA tiles were densely clustered at the surface of not only mica but also fluid POPC membrane, although they differed in density and size of the assembly (**Fig. 3c, 3d, S3c and S3d**). The presence of divalent cations is known to stabilize binding of polyanionic DNA to zwitterionic lipid membranes by electrostatic interactions.[37-39] Binding of 2D DNA nanostructures onto the membranes intermediated by divalent cations without hydrophobic anchoring has been previously reported.[15,16,19] On the other hand, at low concentrations of Mg^{2+} (3 mM) even the DNA tiles containing dod-DEG-A unit could not bind to the membrane (**Fig. 3e, S3e**). However, when dod-DEG groups were introduced into both A and B units, the DNA tiles attached to and assembled on the POPC membrane, even at 3 mM Mg^{2+} (**Fig. 3f, S3f**). Each DNA tile consisting of dod-DEG-A/B and dod-DEG-A/dod-DEG-B has 1 dod-DEG group per 82 and 42 base pairs, respectively. This result shows that, by changing the density of the hydrophobic modifications in the 2D DNA structure, the membrane binding properties can be modulated.

The images showing binding of dod-DEG-DNA tiles on POPC show that the lattice is not well formed and that only a few instances of the characteristic stripe pattern can be observed on the membrane. This is most likely because the assembly of a stable periodic 2D lattice was prevented by diffusion on the fluid membrane. The DNA structures bound to fluid POPC membranes were observed to diffuse and disassemble during AFM imaging, as shown in the supplementary information (**Fig. S4**). The characteristic stripe pattern of constant width (29.9 nm ± 0.4) can be measured also in these cases (**Fig. 4a**, **c**). Height analysis confirms that the 2 nm thick DNA lattice is resting on the 4 nm thick POPC bilayer (**Fig. 4b**).

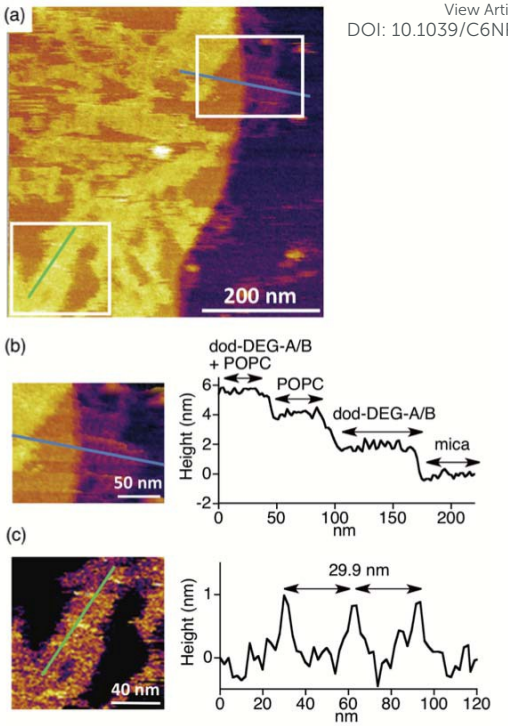

Fig. 4. (a) High resolution AFM image of dod-DEG-A/B tiles on a POPC planar lipid bilayer in 10 mM Tris-HCl (pH 8.0) buffer containing 6 mM of Mg^{2+} (b) Height profile measured along the blue line showing the step heights corresponding to DNA structures and POPC. (c) Height profile measured along the green line in the white box showing a stripe with constant width (29.9 nm).

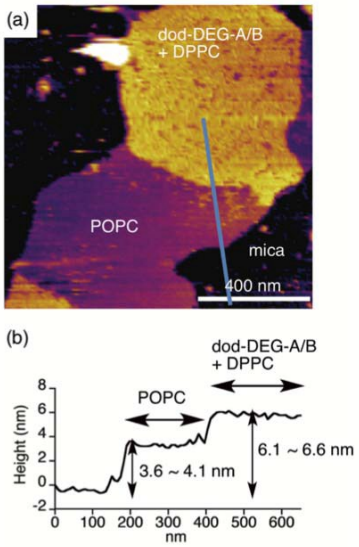

Fig. 5. (a) dod-DEG-A/B tile adsorbed preferentially on the DPPC gel phase patches of a lipid membrane composed of POPC/DPPC (1:1 molar ratio) lipid mixture, in the presence of 6 mM Mg^{2+}. Scale bar, 400 nm. (b) Height profile along the blue line in (a), demonstrating accumulation of DNA tiles on the DPPC patches.

View Article Online
DOI: 10.1039/C6NR07084A

To see effects of the membrane lipid phases on binding of the DNA tiles, we tested the binding of the DNA tiles to gel-phase 1,2-dipalmitoyl-*sn*-glycero-3-phosphocholine (DPPC) lipid membranes. DNA tiles attached to the surface of the DPPC membrane at 6 mM Mg^{2+} regardless of whether DNA tiles had the hydrophobic modifications or not as we show in the Supplement (**Fig. S5**)**.** Remarkably, when we used a 1:1 mixture of DPPC:POPC that contains both gel and fluid phase domains, DNA tiles were localized almost exclusively on the gel-phase DPPC membrane (**Fig. 5, S6, S7**)**.** In a previous study, a DNA origami structure was found to preferentially bind to a liquid ordered phase rather than to a liquid disordered phase in the presence of Mg^{2+}.[11,19,39] Non-fluidic and ordered phases are favorable for binding of DNA nanostructures, most likely because the non-fluidic nature of the membrane minimizes entropic loss of lipid molecules upon the binding of the DNA structures.

Force spectroscopy measurements

The insertion of the hydrophobic tail in the lipid bilayers is expected to affect lipid mobility and the mechanical properties such as viscosity and the bilayer rupture force as in the case of other hydrophobic molecules inserted in the bilayer core.[41,42] To assess how the mechanical properties of a fluid membrane are affected by binding of the amphiphilic 2D DNA lattice, force versus indentation measurements for the DNA-lipid membrane complex were performed. We used the same experimental conditions as for **Fig. 4a**, at 6 mM Mg^{2+}, where the dod-DEG-modified DNA tiles were stably attached to the membrane, while the unmodified DNA tiles could not bind. In these conditions, we could measure force-indentation curves of both the DNA-lipid membrane complex and the bare membrane in the same sample and directly compare them.

Fig. 6a shows a typical force vs indentation approach curve for the DNA-membrane complex on mica. For comparison, indentation curves for mica, POPC bilayer membrane and DNA tile were also measured (**Fig. 6b**). The force-indentation curves of DNA-POPC structure consists of four parts with distinct slopes (labelled I-IV in **Fig. 6a**). The cantilever first contacts and deforms the surface of the DNA which can be seen in the first ~2 nm of the force-indentation curve after the force starts to increase upon contact with the surface (stage I). Then the force curve becomes more dominated by POPC mechanics in the following ~2 nm of indentation (stage II). After that the curve becomes steeper with an almost constant slope, in which the slope is a result of the combination of the membrane and the stiffer underlying mica support (stage III).[43,44] After breakthrough of the POPC membrane (sudden jump in the curve depicted by arrows in **Fig. 6a** and **b**) the tip comes into contact with mica (stage IV). Each slope in the force-indentation curves, which is related to the stiffness of the sample, roughly corresponds to slopes obtained for the reference measurements, as can be seen in **Fig. 6b**. It is difficult to determine from this experiment the interface of the DNA and POPC and hence quantitative calculation of the changes of elastic modulus of the bilayer is difficult by fitting of the curve to the available models for thin films. However comparing the curves for POPC and DNA-POPC one can see changes in the slope; in stages I-II, POPC is becoming less resistant to deformation upon insertion of the DNA tiles, and in contrast, the slope is slightly steeper than for pure POPC in the following 2 nm of indentation (stage III). This complex, multistage behavior of the indentation curve may be explained

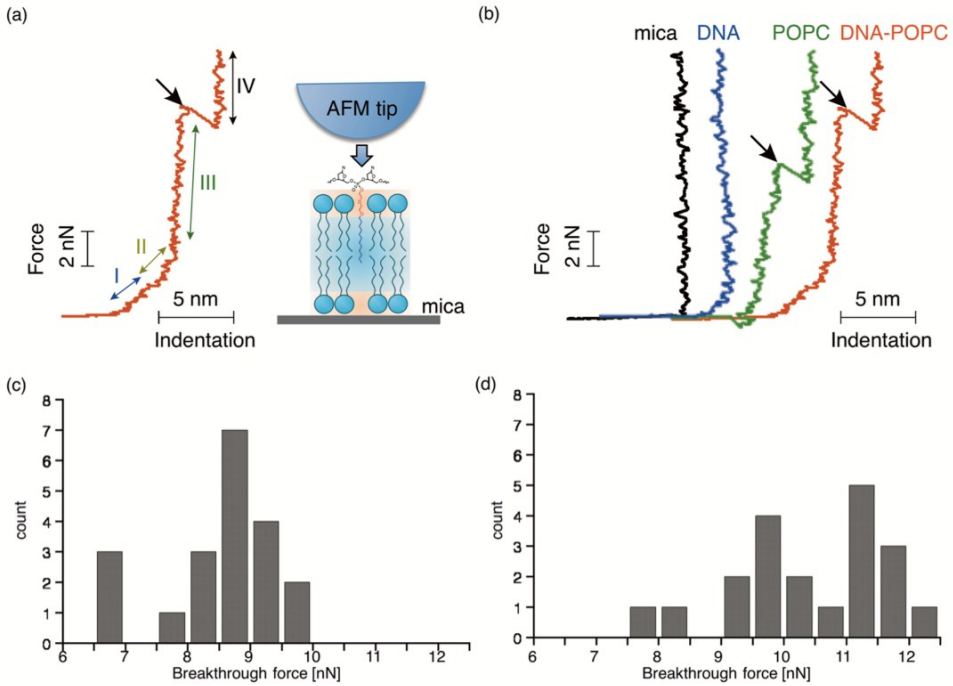

Fig. 6. (a) Typical force vs indentation curves on DNA tiles inserted in POPC bilayers (red), (b) DNA tiles on mica (blue), and DNA tiles-POPC (red), POPC (green). Mica is given as a reference in black. The curves were recorded in the same conditions in Figure 4a. The breakthrough point in the bilayer can be detected as a sudden jump in the force vs. indentation curve depicted by arrows in (a) and (b). Four distinctive regime regions in the indentation are shown by two-headed arrows (stages I, II, III, and IV); (c) and (d) show the distributions of the breakthrough forces for pure POPC bilayers (c) and DNA-POPC (d).

View Article Online
DOI: 10.1039/C6NR07084A

by the asymmetric effect of DNA binding in the bilayer. The dod-DEG tail interacts with the top leaflet of the bilayer, which can be expected to affect the mechanical properties of top and bottom membrane leaflets differently. Changes of the inter- and/or intra-layer interactions possibly result in weakening of either of the leaflets (stage II) and stiffening another leaflet (stage III), which would explain the multistage indentation curve.

Furthermore, the insertion of the tiles has a significant effect on so-called rupture or breakthrough force of the bilayer.[41] The breakthrough force is as the force at which the membrane breaks under the force produced by the tip indentation (depicted by arrows in **Fig. 6a** and **b**). The breakthrough force is a measure of the lipid cohesion and mobility within the membrane**.** The distributions of the breakthrough forces for POPC and DNA-POPC are plotted in **Fig. 6c** and **d**. The breakthrough forces for DNA-POPC membrane (10.5 ± 0.9 nN) shift to higher values as compared with the bare POPC membrane (8.61 ± 1.3 nN). The DNA tiles attached onto the membrane make the POPC membrane more difficult to break through. There are at least two reasons that might explain this. The confinement of the Mg^{2+} ions between the DNA tile and the lipids may enhance the lipid-lipid head-group interactions. Furthermore the insertion of the hydrophobic DNA tails in the bilayer and the confinement of Mg^{2+} at the interface can be expected to reduce lipid mobility, causing a similar effect on the increased rupture force to C_{60} fullerenes inserted in bilayers.[42]

Conclusions

We have demonstrated the assembly of 2D DNA lattices on lipid membranes and showed how the assembly affects the mechanical properties of the membranes. The binding of the DNA structures to membranes is dependent on lipid phase of the membrane, concentration of Mg^{2+} cation, and the amphiphilic modifications to the DNA. In particular, binding of DNA structures to fluid POPC planar lipid bilayers could be controlled by the introduction of dod-DEG groups. The modified DNA structures do not aggregate in solution. The formation of the 2D DNA lattices on the membrane was clearly visualized by AFM. We found that the bound DNA structures enhanced the mechanical stability of the membrane, producing an increase of 20% in the bilayer rupture force, demonstrating a potential ability of the amphiphilic DNA to modulate physical properties of lipid membranes. Interestingly our results show that the tiles assemble preferentially on gel phase lipids in coexisting fluid/gel phases. This result could be useful for the selective assembly of DNA nanostructures in less fluid domains of the cell membrane, for *e.g.* targeting a specific cellular signaling pathway in therapeutic interventions. The controlled binding of DNA structures to lipid membranes is an important basis for applications where DNA nanostructures and assemblies would exert functions related to cell membranes both in medical/biological and synthetic biology applications, such as designed cytoskeletal networks, membrane-deformation, drug-delivery systems, and biochemical reaction cascades.

Experimental

Synthesis of dod-DEG-DNA: The synthesis of dod-DEG-DNA was carried with on Applied Biosystem 3400 DNA/RNA synthesizer using an ultramild phosphoramidite method. To apply the ultra-mild deprotection condition, phenoxyacetyl protected dA and 4-isopropyl-phenoxyacetyl protected dG (Glen Res) were used as monomers and phenoxyacetic anhydride was used in Cap A solution. Nucleoside phosphoramidites containing a dod-DEG group were synthesized according to previously reported procedure. Details of the phosphoramidites synthesis were described in the supporting materials. The synthesized DNAs were cleaved form the resin and deprotected by the ultra-mild condition, *i.e.* treating with 28% NH_3 aqueous at room temperature for 2 h. The resulting mixtures were purified by reverse-phase HPLC on a CHEMCOBOND 5-ODS-H column (10 × 150 mm) eluting with 5–45 % (40 min) or 20–80 % (60 min) acetonitrile in 0.1 M triethylammonium acetate (TEAA), pH 7.0, at a flow rate 3.0 mL/min.

Small unilamellar vesicles (SUVs) preparation for SPR: 10 mM 1-palmitoyl-2-oleoyl-*sn*-glycero-3-phosphocholine (POPC, NOF corporation) in chloroform (1 mL) was evaporated in glass vial to create a film on the surface. The vial was further dried under a vacuum 2 h, and 1 mL of phosphate-buffered saline was then added to vial. The vial was then vortexed vigorously and was freeze-thawed five times. The suspension was then extruded through two 50 nm polycarbonate filters in Avestin Lipofast Basic extrusion apparatus to give translucent solution of 50 nm vesicles. The prepared SUVs were diluted to a final lipid concentration of 0.5 mM and were used for SPR analysis.

SUVs preparation for AFM: 10 mM POPC, 10 mM 1,2-dipalmitoyl-*sn*-glycero-3-phosphocholine (DPPC, NOF corporation), or 10 mM POPC/DPPC (1:1 molar ratio) in chloroform (1 mL) was evaporated in glass vial to create a film on the surface. The vial was further dried under a vacuum 2 h, and 1 mL of 10 mM Tris-HCl (pH 8.0) buffer was then added to the vial. The suspension was then vortexed vigorously and was sonicated for 30 min at 40% of the duty cycle by sonifier 250 (Branson, USA). The prepared SUVs were diluted to a final lipid concentration of 1 mM and were used for AFM.

Immobilization of POPC-SUV on a SPR Sensor Chip and SPR Analysis: The interaction between amphiphilic DNA and lipid bilayer membrane was assessed by SPR measurements using a Biacore 3000 system using sensor chip L1 (Biacore). For immobilization of POPC-SUVs, the sensor chip was cleaned with 50 µL of 40 mM *n*-octyl-β-glucoside at a flow rate 10 µL/min and then POPC-SUVs were injected at flow rate of 2 µL/min for 15 min at 25 °C. After injection of the SUVs, 10 mM NaOH was injected for 2.5 min at a flow rate of 2 µL/min to remove the multiple layers of lipids. Bovine serum albumin (20 µL, 100 mg/mL) was then injected at a flow rate of 2 µL/min to block the nonspecific binding sites. In order to analyze the binding affinity of dod- or dod-DEG-DNAs to the POPC

membrane, 20 µL of dod- or dod-DEG-DNAs (5 µM) were injected into the POPC-SUV immobilized sensor chip. 20 µL of complementary DNA strand (5 µM, purchased from Invitrogen) was subsequently injected to monitor the DNA hybridization. After each injection, 20 µL of the buffer was injected to observe the dissociation of the DNAs from the lipid membrane. At the end of each binding assay, a 40/60 (v/v) mixture of isopropanol and 50 mM NaOH were injected at flow rate 10 µL/min to regenerate the sensor chip surface.

Assembly of the DNA tiles: DNA tile was prepared according to previously reported procedure (supporting information).[36] The concentration of all oligonucleotides was adjusted to 100 µM by ultraviolet absorption at 260 nm with NanoVue (GE Healthcare). The strands of each tile unit were mixed and diluted to 1 mM in Tris-acetate-EDTA (1 × TAE) buffer containing $Mg(OAc)_2$ (12.5 mM). The solution was annealed by heating at 95 °C and slowly cooling to 30 °C during 6 h in TP100 thermal cycler (TAKARA BIO INC.). Separately prepared DNA tiles A and B were mixed and annealed from 45 °C to 10 °C during 13 h.

AFM experiments: 50 µL of 1 mM SUVs solutions with 2 mM $CaCl_2$ were spotted onto freshly cleaved mica and incubated for 2 h at room temperature. After rinsing the lipid-coated mica with 10 mM Tris-HCl (PH 8.0) buffer with 3–12.5 mM $Mg(OAc)_2$, the DNA tiles were spotted onto the lipid-coated mica and incubated for 1 h at 4 °C, then rinsed with 10 mM Tris-HCl (pH 8.0) buffer with 3–12.5 mM $Mg(OAc)_2$. AFM experiments were performed with MFP-3D BIO™ (OXFORD Instruments Co., Ltd., UK) with OMCL-TR800PSA and RC800PSA cantilever tips (OLYMPUS Optical Co., Ltd.) with 0.57 and 0.38 Nm^{-1} spring constant, respectively. All images were taken in 10 mM Tris-HCl (pH 8.0) buffer with 3–12.5 mM $Mg(OAc)_2$ at room temperature at a scan speed of 0.5–1.5 Hz. Force curve measurements were performed using the same conditions to the AFM imaging described above. The concentration of $Mg(OAc)_2$ was fixed to 6 mM. All force curves were acquired using OMCL-TR800PSA cantilever tips with a velocity of 100 nm/s. Individual spring constants were calibrated using the thermal noise method. To calculate the inverse optical lever sensitivity (InvOLS), force curves were taken on mica before and after force curves acquisition of the samples. Breakthrough forces (rupture forces) were obtained from the force value where sudden jump of the indentation in the curve was observed.

Acknowledgements

Funding from the collaboration grant JSPS Core-to-core programme is acknowledged. This work was supported by a Grant-in-Aid for Challenging Exploratory Research 15K12746 (C.D.) from the Japan Society for the Promotion of Science (JSPS) and by Precursory Research for Embryonic Science and Technology, Japan Science and Technology Agency (PRESTO-JST). SC acknowledges discussions with Jonathan Bath (Oxford Physics).

Notes and references

View Article Online
DOI: 10.1039/C6NR07084A

1 P. W. K. Rothemund, *Nature*, 2006, **440**, 297-302.
2 V. Linko and H. Dietz, *Curr. Opin. Biotechnol.*, 2013, **24**, 555-561.
3 T. Torring, N. V. Voigt, J. Nangreave, H. Yan and K. V. Gothelf, *Chem. Soc. Rev.*, 2011, **40**, 5636-5646.
4 F. Zhang, J. Nangreave, Y. Liu and H. Yan, *J. Am. Chem. Soc.*, 2014, **136**, 11198-11211.
5 A. V. Pinheiro, D. R. Han, W. M. Shih and H. Yan, *Nat. Nanotechnol.*, 2011, **6**, 763-772.
6 M. R. Jones, N. C. Seeman and C. A. Mirkin, *Science*, 2015, **347**, 1260901.
7 M. Carquin, L. D'Auria, H. Pollet, E. R. Bongarzone and D. Tyteca, *Prog. Lipid Res.*, 2016, **62**, 1-24
8 K. Simons and M. J. Gerl, *Nature reviews. Molecular cell biology*, 2010, **11**, 688-699.
9 A. Anishkin and C. Kung, *Proc. Natl. Acad. Sci. U. S. A.*, 2013, **110**, 4886-4892.
10 A. Kaufmann, V. Beier, H. G. Franquelim and T. Wollert, *Cell*, 2014, **156**, 469-481.
11 M. Langecker, V. Arnaut, J. List and F. C. Simmel, *Acc. Chem. Res.*, 2014, **47**, 1807-1815.
12 A. Czogalla, H. G. Franquelim and P. Schwille, *Biophys. J.*, 2016, **110**, 1698-1707.
13 Y. Suzuki, M. Endo and H. Sugiyama, *Acs Nano*, 2015, **9**, 3418-3420.
14 M. Kwak and A. Herrmann, *Chem. Soc. Rev.*, 2011, **40**, 5745-5755.
15 Y. Suzuki, M. Endo and H. Sugiyama, *Nature communications*, 2015, **6**, 8052.
16 Y. Suzuki, M. Endo, Y. Yang and H. Sugiyama, *J. Am. Chem. Soc.*, 2014, **136**, 1714-1717.
17 K. Börjesson, E. P. Lundberg, J. G. Woller, B. Nordén and B. Albinsson, *Angew. Chem. Int. Ed.*, 2011, **50**, 8312-8315.
18 E. P. Lundberg, B. B. Feng, A. S. Mohammadi, L. M. Wilhelmsson and B. Nordén, *Langmuir*, 2013, **29**, 285-293.
19 A. Czogalla, E. P. Petrov, D. J. Kauert, V. Uzunova, Y. Zhang, R. Seidel and P. Schwille, *Faraday Discuss.*, 2013, **161**, 31-43.
20 A. Czogalla, D. J. Kauert, H. G. Franquelim, V. Uzunova, Y. Zhang, R. Seidel and P. Schwille, *Angew. Chem. Int. Ed. Engl.*, 2015, **54**, 6501-6505.
21 J. List, M. Weber and F. C. Simmel, *Angew. Chem. Int. Ed. Engl.*, 2014, **53**, 4236-4239.
22 J. R. Burns, E. Stulz and S. Howorka, *Nano Lett*, 2013, **13**, 2351-2356.
23 M. Langecker, V. Arnaut, T. G. Martin, J. List, S. Renner, M. Mayer, H. Dietz and F. C. Simmel, *Science*, 2012, **338**, 932-936.
24 S. Kocabey, S. Kempter, J. List, Y. Z. Xing, W. Bae, D. Schiffels, W. M. Shih, F. C. Simmel and T. Liedl, *ACS Nano*, 2015, **9**, 3530-3539.
25 Y. Yang, J. Wang, H. Shigematsu, W. M. Xu, W. M. Shih, J. E. Rothman and C. X. Lin, *Nat. Chem.*, 2016, **8**, 476-483.
26 S. D. Perrault and W. M. Shih, *ACS Nano*, 2014, **8**, 5132-5140.
27 C. Dohno, T. Shibata, M. Okazaki, S. Makishi and K. Nakatani, *Eur. J. Org. Chem.*, 2012, 5317-5323.
28 S. Makishi, T. Shibata, M. Okazaki, C. Dohno and K. Nakatani, *Bioorg. Med. Chem. Lett.*, 2014, **24**, 3578-3581.
29 T. Shibata, C. Dohno and K. Nakatani, *Chem. Commun.*, 2013, **49**, 5501-5503.
30 C. Dohno, K. Matsuzaki, H. Yamaguchi, T. Shibata and K. Nakatani, *Org. Biomol. Chem.*, 2015, **13**, 10117-10121.
31 J. F. Nagle and S. Tristram-Nagle, *Biochim. Biophys. Acta*, 2000, **1469**, 159-195.
32 G. Stengel, R. Zahn and F. Höök, *J. Am. Chem. Soc.*, 2007, **129**, 9584-9585.

View Article Online
DOI: 10.1039/C6NR07084A

33 A. Bunge, M. Loew, P. Pescador, A. Arbuzova, N. Brodersen, J. Kang, L. Dähne, J. Liebscher, A. Herrmann, G. Stengel and D. Huster, *J. Phys. Chem. B*, 2009, **113**, 16425-16434.
34 R. V. Stahelin, *Mol. Biol. Cell*, 2013, **24**, 883-886.
35 V. Hodnik and G. Anderluh, *Methods Mol. Biol.*, 2013, **974**, 23-36.
36 E. Winfree, F. R. Liu, L. A. Wenzler and N. C. Seeman, *Nature*, 1998, **394**, 539-544.
37 V. G. Budker, A. A. Godovikov, L. P. Naumova and I. A. Slepneva, *Nucleic Acids Res.*, 1980, **8**, 2499-2515.
38 S. Gromelski and G. Brezesinski, *Langmuir*, 2006, **22**, 6293-6301.
39 A. Kato, A. Tsuji, M. Yanagisawa, D. Saeki, K. Juni, Y. Morimoto and K. Yoshikawa, *The Journal of Physical Chemistry Letters*, 2010, **1**, 3391-3395.
40 P. A. Beales and T. K. Vanderlick, *J. Phys. Chem. B*, 2009, **113**, 13678-13686.
41 S. Garcia-Manyes and F. Sanz, *Biochim. Biophys. Acta*, 2010, **1798**, 741-749.
42 J. Zhou, D. Liang and S. Contera, *Nanoscale*, 2015, **7**, 17102-17108.
43 K. Voitchovsky, S. A. Contera, M. Kamihira, A. Watts and J. F. Ryan, *Biophys. J.*, 2006, **90**, 2075-2085.
44 E. K. Dimitriadis, F. Horkay, J. Maresca, B. Kachar and R. S. Chadwick, *Biophys. J.*, 2002, **82**, 2798-2810.